JOURNAL OF MATERIALS SCIENCE 33 (1998) 2137–2145

The effects of aluminium composition on the mechanical properties of reactivity sputtered TiAlN films

DING-FWU LII
Department of Electrical Engineering Chinese Naval Academy Kaohsiung, Taiwan 813
E-mail: dflii@mail.cna.edu.tw

TiAlN films were deposited on tool materials through an r.f. bias reactive sputtering process. The effects of the aluminium composition in the films on the hardness, oxidation resistance and wear properties were studied. The results indicated that both the aluminium composition and cutting speed had substantial effects on wear resistance. The oxide phases formed at elevated cutting temperatures, especially alumina, had important effects on the cutting performance. An optimum improvement of nine times in wear resistance compared to uncoated tools, was observed. © *1998 Chapman & Hall*

1. Introduction

Cutting-tool materials require extremely good mechanical, thermal and chemical properties at elevated temperatures due to the harsh cutting conditions in use. Several hard ceramic coatings have previously been developed for high-speed machining and longer tool life [1]. However, some problems with the commercialized cutting tool materials are still unsolved. For example, TiC and TiN begin to oxidize at temperatures of 400 and 500 °C, respectively [2]. Ti(C, N)-coated inserts undergo serious wear at crater faces under continuous cutting [3], and diamond reacts extensively with IVB and VIII elements and wears rapidly during machining of mild steels [4].

Titanium aluminium nitride was successfully developed as a potential coating material in less than a decade. Its cutting performance was reported to be superior to that of other conventional binary coatings and could be used at significantly higher cutting speeds [2, 3, 5, 6].

Most of the previous reports on TiAlN films concentrated on a Ti/Al ratio of 1:1 (i.e. $Ti_{0.5}Al_{0.5}N$) [2, 3, 5–9]. Some researchers investigated the hardness and Young's modulus of TiAlN films with different aluminium contents [10, 11], however, the correlation between the aluminium composition and the mechanical properties of TiAlN films is still not clear.

The effects of nitrogen gas flow rate and r.f. bias on the microstructure and mechanical properties of TiAlN films were previously reported [12, 13]. The effects of aluminium content on the oxidation behaviour of TiAlN films were also investigated [14]. This report is a continuation of a series of studies on the effect of aluminium composition on TiAlN films. In the present work, the TiAlN films were deposited by magnetron reactive sputtering with an r.f. bias. Titanium aluminium alloys with different Ti/Al ratios were used as targets for controlling the aluminium composition in TiAlN films. The effects of aluminium content on the mechanical and cutting properties of TiAlN films were investigated.

2. Experimental procedure

2.1. Sample preparation

Titanium aluminium nitride films were deposited on SKH51 (chemical composition (wt%) 0.8 C; 4.8 Mo, 6.1 W, 1.9 V, 0.28 Si, 0.27 Mn, 0.02 P, 0.01 S, 0.2 Ni, balance Fe)HSS discs (diameter $20 \times 3\ mm^2$) by reactive d.c. magnetron sputtering. The HSS substrates were annealed (860 °C), quenched from 1200 °C and then tempered at 550 °C. A Rockwell hardness of 64 HRC was obtained after the heat treatment. The substrates were then finely polished to 1 μm, degreased, ultrasonically cleaned in alcohol for 3 min and subsequently blown dry in flowing nitrogen gas. The targets used in this study were titanium–aluminium alloys (diameter $7.62 \times 0.635\ cm^2$, Plasmaterial Inc. USA) with Ti/Al (at%) ratios of 100/0, 90/10, 75/25, 50/50, and 40/60.

Sputtering was conducted in a mixed argon–nitrogen gas atmosphere with a target to substrate distance of 4 cm. A diffusion pump coupled with rotary pump was used to achieve an ultimate pressure of 10^{-5} torr (1 torr = 133.322 Pa) before introducing gas mixtures of argon (99.999%) and nitrogen (99.9995%). The substrates were presputtered by a r.f. argon discharge at $1.33\ N\,m^{-2}$ with an energy density of $0.4\ W\,cm^{-1}$ for 10 min prior to film deposition for cleaning purposes.

The TiAl target was cleaned by sputtering in argon gas (2.67 $N m^{-2}$) for 5 min before depositing films. The total pressure and the flow rate of argon were maintained at 0.8 $N m^{-2}$ and 20 $l min^{-1}$, respectively, during deposition. An r.f. power supply was used for establishing a negative bias voltage of -80 V [13]. The cathode current and the substrate temperature were controlled at 0.7 A and 350 °C. The flow rate of nitrogen gas varied in the range of 0–10 $l min^{-1}$ depending on the aluminium content. The film thickness was controlled at 2 μm. Deposited samples were cooled down in an argon atmosphere to below 100 °C before venting the system.

2.2. Characterization of TiAlN films

The film thickness was measured by an α-step (Tencor 250, USA) apparatus. The deposition rate was calculated from the film thickness and deposition time.

The lattice spacing of the films was analysed using an X-ray diffractometer (Rigaku D/Max-IV, Japan) using Cu*K* radiation with a speed of 4 ° min^{-1} from 30 °–80 °. A glancing XRD (GXRD, Rigaku DMAX 2500, Japan) was used for determining the oxidized phases in TiAlN films. Scanning electron microscopy (SEM) was used for microstructural analysis.

Auger electron spectroscopy (AES) was used for analysing the chemical composition of films based on a previous report by Shew and Huang [15]. Samples were sputtered by argon ions at 3 keV before conducting AES analysis for eliminating possible surface contamination.

2.3. Mechanical properties

The Vickers hardness was measured using a microhardness indentor (Matsuzawa NTX70) at 25 g. The possible influence from the substrate was neglected due to the measured surfacial indent diagonal being much less than the film thickness [16]. Each data point was the average of more than 10 measurements.

The wear resistance was evaluated by a wear-testing apparatus (Optimol Inc. model SRV) with a chromium steel ball as the counter part. An oscillatory sliding motion was performed against the test sample at a frequency of 50 Hz. The depth and width of wear scars were carefully measured as an indication for wear resistance.

The adhesive strength was determined by a scratch test apparatus (Romulus II Universal Tester, Quad Inc.) using a Rockwell diamond stylus with a tip radius of 125 μm. The test was operated at a loading rate of 1 $N s^{-1}$ with a scratch length of 8 mm. Both acoustic emission and light microscopic techniques were used to correlate the friction, appearance of scratches and the critical scratch load.

The crater wear [3, 17] resistance of coated carbide tools (Mitsubishi Metal, ISO specification TPMN160308, UTi20T, Chemical composition (vol%): 12–15 Co, 18–20 TiC + TaC, balanced WC) was tested on a CNC lathe (Leadwell LTC-10P) by cutting grey cast iron. The depth of cut and feed rate were 1–4 mm and 0.1–0.4 mm rev^{-1}, respectively. The cutting speed varied from 50–200 m min^{-1}. Samples were ultrasonically cleaned in acetone and the crater depth was carefully measured after a cutting distance of 1640 m.

3. Results and discussion

3.1. Microhardness, optimum nitrogen gas flow rate and chemical compositions

The hardness of TiAlN films deposited from targets with different Ti/Al ratios was measured as a function of nitrogen flow rate (Fig. 1). Results indicated that the hardness initially increased with nitrogen flow rate and then decreased. In addition, the value of optimum hardness increased and occurred at a higher nitrogen flow rate as the aluminium content increased [10].

The optimum hardness occurred in a range of nitrogen gas flow which was higher than the critical value (Fig. 1) [12]. This was attributed to the occurrence of smaller grain size, better adhesion and wear resistance in this range [12]. This observation was different from TiN films in which the optimum hardness occurred at certain nitrogen gas flow and then dropped dramatically as the nitrogen flow rate exceeded the critical value [18, 19]. The range of nitrogen flow for obtaining optimum hardness also became wider as the composition of aluminium in targets increased (Fig. 1). This wide range makes the fabrication of high-hardness TiAlN films easier and more controllable.

The TiAlN films with optimum hardness were analysed by AES quantitative analysis and the results were compared with the theoretical compositions calculated from the compositions in the target alloys (Fig. 2). A good agreement between the experimental and theoretical values was observed. Because the theoretical aluminium composition in (TiAl)N is half of its composition in the TiAl target, the samples sputtered from TiAl target alloys with aluminium contents (at %) of 0, 10, 25, 50 and 60 were designated as A0, A5, A12.5, A25 and A30 separately. Sample codes are represented in Table I.

The microhardness was also represented as a function of aluminium composition in TiAlN films as shown in Fig. 3. The results indicated that a maximum value of 3800 $kg mm^{-2}$ was obtained at 25 at % Al.

It was previously reported that the hardness of nitrides and carbides was directly correlated to their bonding energy and interatomic spacing, and was also influenced by the valence electron concentration (VEC) per unit cell [11]. The values of VEC were affected by the stoichiometric composition of individual elements and the composition of vacancies in TiAlN films [20]. The valence electron concentrations of TiAlN films were plotted together with microhardness as a function of aluminium content as shown in Fig. 3.

Results of Fig. 3 indicated that the VEC values of TiAlN films linearly decreased with aluminium content. This was probably due to more titanium atoms (Ti^{4+}) being replaced by relatively smaller

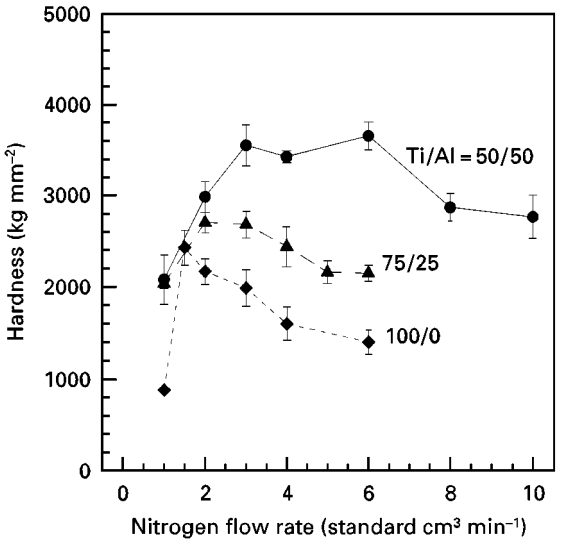

Figure 1 Hardness of TiAlN films deposited from targets with different Ti/Al ratios and various nitrogen flow rates.

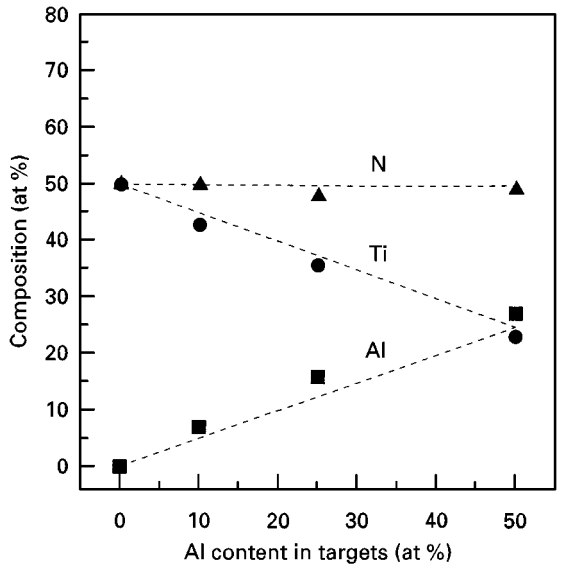

Figure 2 AES quantitative analysis of TiAlN films versus the aluminium composition in targets.

TABLE I Designation and composition of samples used in this study

Sample code	Al composition in target alloys (at %)	Theoretical composition of Al in TiAlN films (at %)
A0	0	0
A5	10	5
A12.5	25	12.5
A25	50	25
A30	60	30

aluminium atoms (Al^{3+}) as the aluminium composition increased [21]. Following a similar calculation by Konig *et al.* [20], the VEC value corresponding to 25 at % Al was calculated as 8.5. This value was in good agreement with a previous study by Konig *et al.* [20], who reported that an optimum hardness could be obtained in a valence electron concentration range of 8.4–8.6 for ternary coatings.

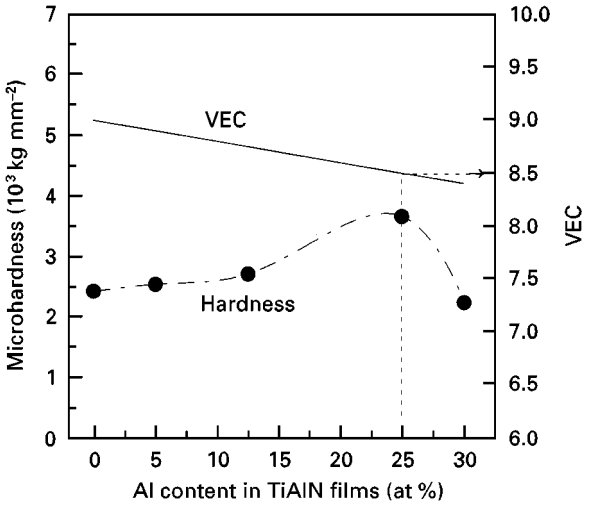

Figure 3 Hardness and valence electron concentration (VEC) versus the aluminium composition in TiAlN films.

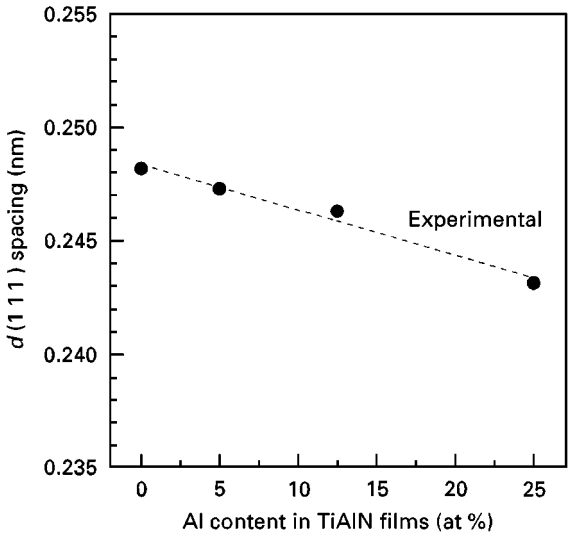

Figure 4 Measured d(1 1 1) spacing versus the aluminium composition in TiAlN films.

The microhardness of TiAlN films degraded dramatically as the aluminium composition in TiAlN exceeded 25 at %. This was probably due to its lack of crystallinity and oversaturation of aluminium [14].

The effects of aluminium addition on the interatomic spacing was investigated by measuring d(1 1 1) spacing in TiAlN films as a function of aluminium contents (Fig. 4). Results from X-ray diffraction revealed that the d(1 1 1) spacing decreased linearly with the aluminium content due to the substitution of relatively larger titanium atoms by smaller aluminium atoms [21]. This tendency was in agreement the VEC values shown in Fig. 3.

3.2. Wear test

The depth and volume of wear scars after the SRV test for 30 min were measured as shown in Fig. 5. Results in Fig. 5 reveal that the wear resistance of the HSS substrate was greatly improved by the TiAlN coating. In addition, the depth and volume of wear scars in TiAlN films invariably decreased with increasing

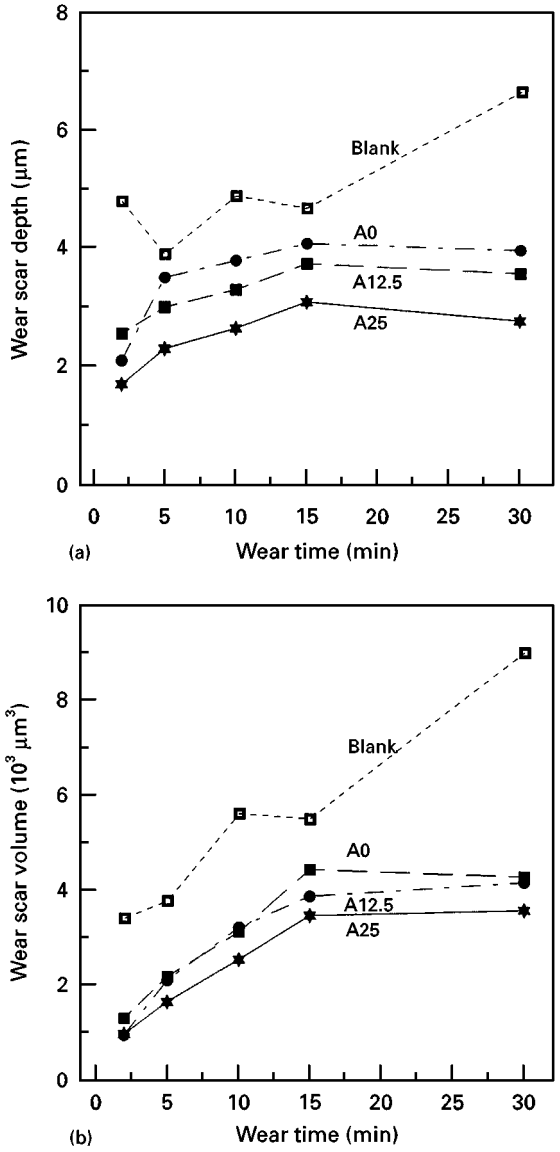

Figure 5 Depth and volume of wear scar in TiAlN films versus wear time.

aluminium. This trend is similar to results shown in Fig. 3 which also indicated an increase in hardness upto 25% Al.

Both mechanical properties and chemical stability have been reported to have a great influence on the wear resistance of TiAlN films [12]. The contact temperature resulting from frictional energy dissipation in relative motion was calculated following an equation derived by Cowan and Winer [22]. The calculated contact temperature on the tool surface during the SRV test was considerably lower than the reported oxidation temperatures of TiN or TiAlN [2]. The wear behaviour of test samples was, therefore, probably controlled by the mechanical property and not the chemical stability.

3.3. Oxidation and diffusion in TiAlN films

The GXRD patterns of TiAlN films with various aluminium contents after oxidizing at 800 °C for 1 h in air are shown in Fig. 6. Results indicated that the TiN-coated HSS (sample code A0) was completely oxidized to form Fe_2O_3. A trace of TiO_2 phase was also detected.

No iron oxide phase was observed in TiAlN-coated samples which strongly suggested an excellent oxidation resistance. The intensity of Al_2O_3 peaks invariably increased with the aluminium content except for A30, in which no obvious crystalline phase was observed. In addition, the TiO_2 was gradually converted into TiO with the increase of aluminium.

The surfaces of oxidized samples were examined by SEM as shown in Fig. 7. The structure of the oxidized surface in A0 appeared loose and porous (Fig. 7a). More dense, grainy and needle-like structures occurred with increasing aluminium contents (Fig. 7b–d). Results by EDS analysis indicated that iron and oxygen were two major compositions in A0 which suggested the formation of iron oxide. Titanium, oxygen and aluminium, but no iron, were detected in TiAlN-coated samples which was in agreement with the XRD results of Fig. 6.

The AES depth profile of coated samples oxidized at 800 °C for 1 h in air are shown in Fig. 8. The aluminium atoms in the films had obviously diffused towards the outer surfaces of the samples after heat treatment. This was probably due to the strong affinity of aluminium for oxygen and its relatively small atomic size. Similar results have been reported by McIntyne *et al.* [23].

The depth profile of oxygen in A0 appeared uniform, which suggested a severe oxidation has occurred after heat treatment. In order to investigate further the oxidation resistance of films, the diffusion depth of oxygen in different samples was plotted from Fig. 8 (Fig. 9). Results showed that the diffusion depth of oxygen decreased with the composition of aluminium in films and reached a minimum value at A25. The penetration depth of oxygen increased slightly as the aluminium content exceeded 25 at %.

The results in Figs 8 and 9 suggested a counter-diffusion of oxygen towards the inner part of samples while the aluminium diffused towards the sample surface. The formation of alumina probably played an essential role for preventing further oxidation. The location of alumina does not necessarily depend on the sample surface, but on the diffusion rates of aluminium and oxygen atoms in the films. The formation of TiO, TiO_2 and iron oxide of TiAlN films (Fig. 6) probably also effects the penetration depth of oxygen, because the diffusion rate of oxygen was reported to be different in different oxides [23]. In samples containing low aluminium contents (A5), the alumina formed at the interior of TiAlN films and resulted in relatively low oxidation resistance (in Fig. 8) [24, 25].

3.4. Abrasive and chemical wear

Abrasive and chemical wear have been reported as the two major wear mechanisms for the cutting tools [21, 26, 27]. By substituting the hardness and geometric factors of machined material and test samples, applied load, and cutting distance into equations derived by Kramer and Judi [26] and Rabinowicz

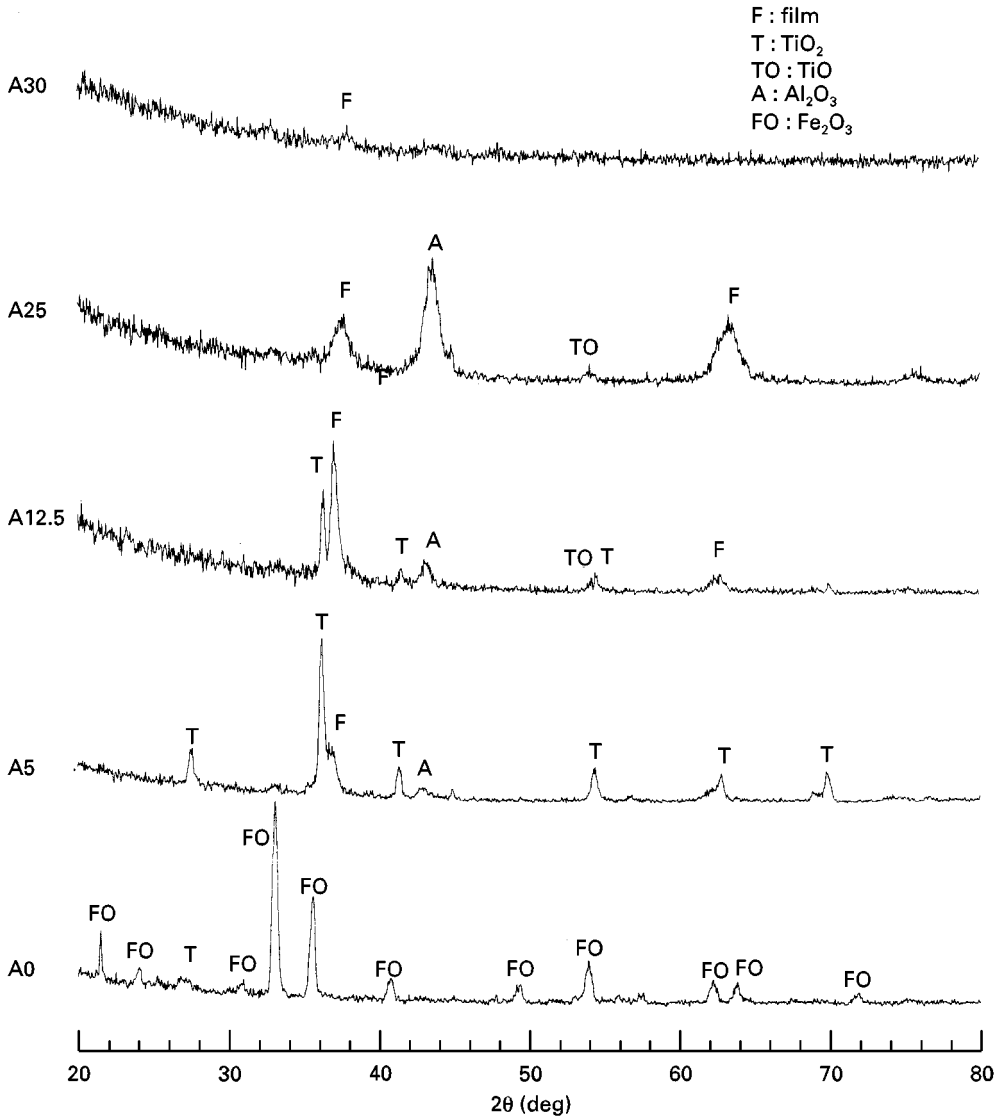

Figure 6 Glancing XRD patterns of TiAlN films after oxidizing at 800 °C, 1 h.

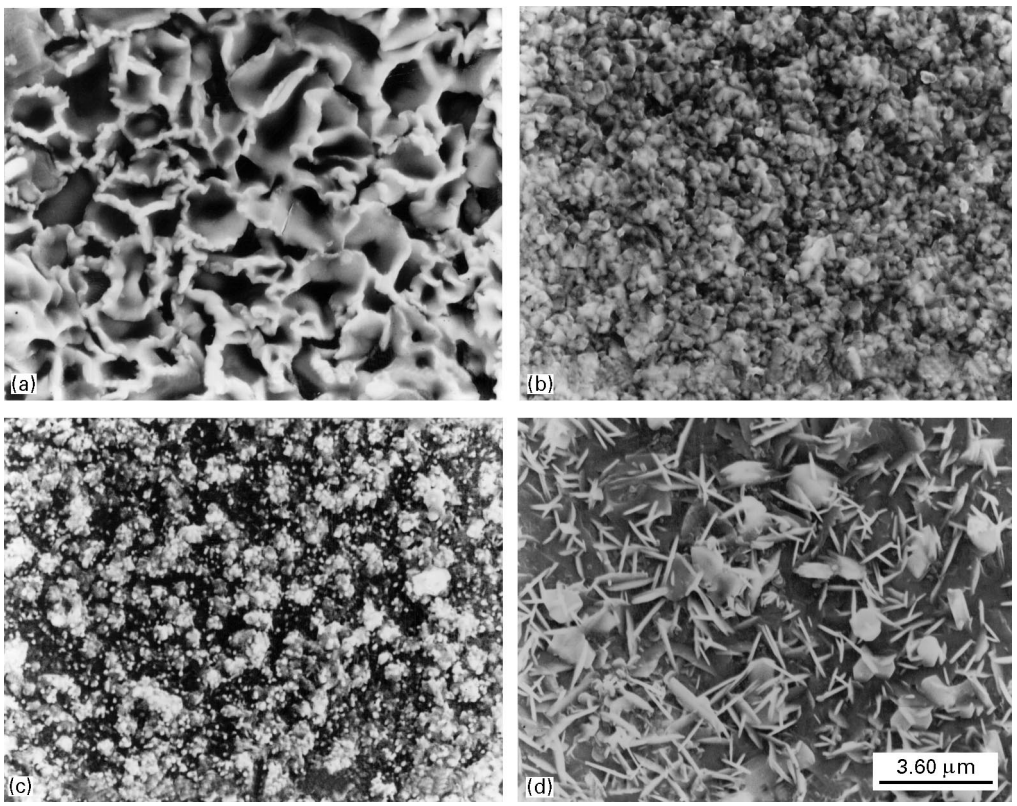

Figure 7 Scanning electron micrographs showing the surfaces of (a) A0, (b) A5, (c) A12.5, (d) A25 films. Samples were oxidized at 800 °C, 1 h.

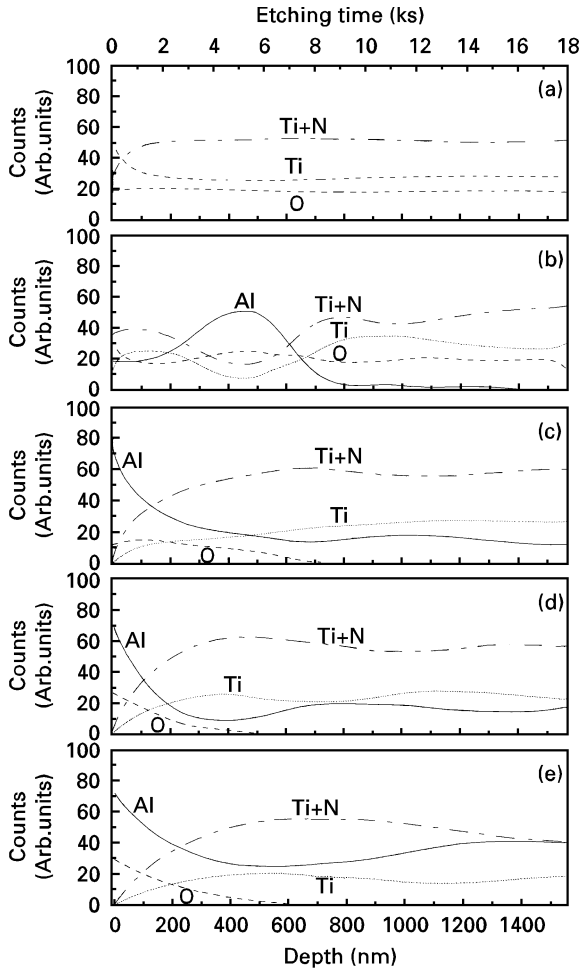

Figure 8 AES depth profile of (a) A0, (b) A5, (c) A12.5, (d) A25, (e) A30 films. Samples were oxidized at 800 °C, 1 h.

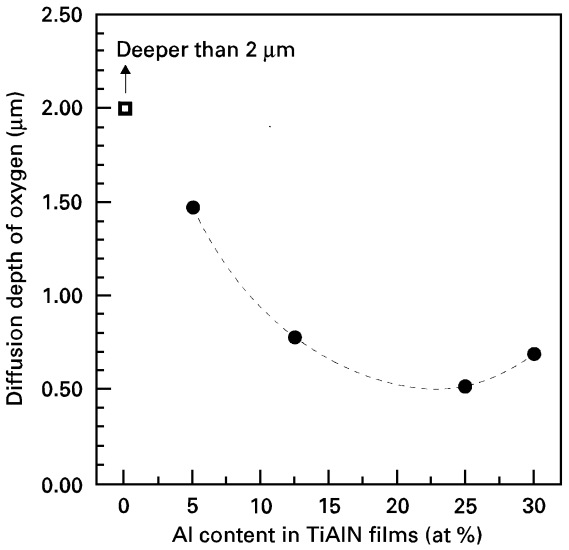

Figure 9 Diffusion depth of oxygen versus the aluminium in TiAlN films. Samples were oxidized at 800 °C, 1 h.

[28], the abrasive wear rates of different materials could be represented as a function of cutting temperature (Fig. 10a). Titanium carbide was used as a base material in Fig. 10.

Based on Henry's law, the chemical wear rates could also be calculated following equations derived by Kramer and Judi [26] considering the free energy

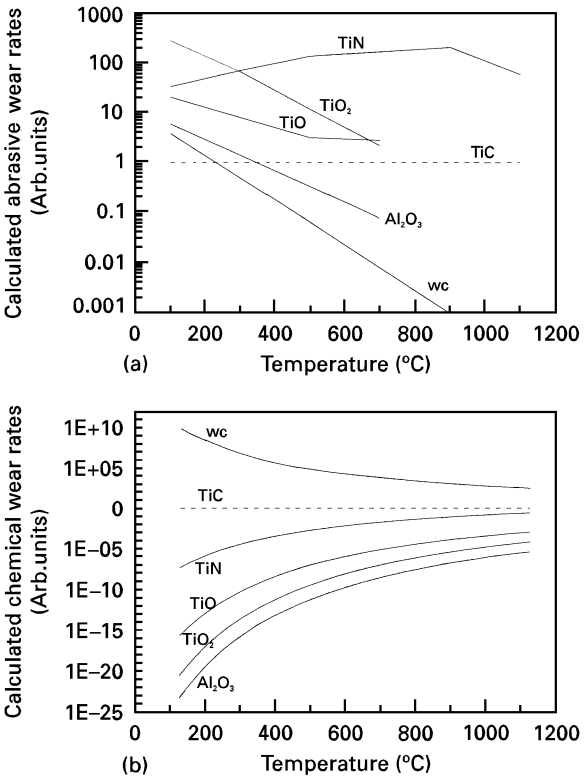

Figure 10 (a) Predicted abrasive wear rates and (b) chemical wear rates of selected materials relative to TiC at various temperatures.

of formation, molar fraction, and excess free energy of each species (Fig. 10b).

3.5. Adhesive strength

The adhesive strength of films containing various aluminium compositions were determined with the results shown in Fig. 11. The critical scratch load invariably decreased with the increasing aluminium content.

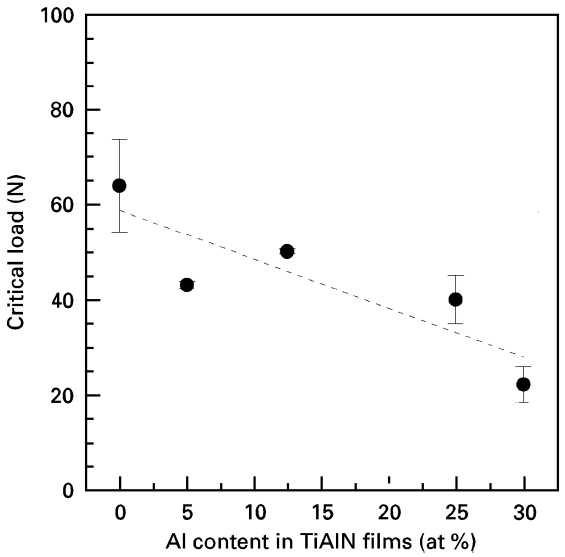

Figure 11 The critical scratch load versus the aluminium composition in TiAlN films.

3.6. Field cutting test

The crater wear depth of TiAlN-coated tools with various aluminium compositions at different cutting speeds were measured and the results were compared with that of uncoated tools (Fig. 12). The wear properties of tools were substantially enhanced by the TiAlN coatings, no matter what aluminium compositions were used. This improvement is especially marked at medium cutting speeds (100 and 150 m min^{-1}).

In order to investigate the effects of film coating on tool life, the results of wear resistance shown in Fig. 12 were expressed in the ratios of coated tools/uncoated tools versus cutting speed (Fig. 13). The tool life was obviously enhanced by film coating. The improvement due to coating was a function of cutting speed and aluminium composition. At relatively low (50 m min^{-1}) and high (200 m min^{-1}) cutting speeds, no obvious difference between coated and uncoated tools was observed. An optimum enhancement of nine times in wear resistance was noted at A12.5 samples at 100 m min^{-1}.

It was formerly reported that tremendous heat could be produced due to friction and plastic deformation during machining [29]. By substituting the cutting conditions into a relationship derived by Shaw [27], the corresponding cutting temperatures for cutting speeds of 50, 100, 150 and 200 m min^{-1} were calculated as 680, 830, 950 and 1050 °C, respectively.

Previous study indicated that, as the cutting temperature exceeded 723 °C, the α-Fe in the machined material (grey cast iron) started to transform into γ-Fe which has strong affinity with carbon in cutting tool material [30]. This was probably why poor wear resistance was observed in uncoated tool material when the cutting speed exceeded 150 m min^{-1}.

The enhancement of wear resistance was particularly phenomenal at medium cutting speeds of 100 and 150 m min^{-1}. The enhancement in coated-samples was in the order medium Al (A12.5 and A25) > low Al (A5) > high Al (A30) > no Al (TiN, A0) > uncoated tools at all cutting speeds. This

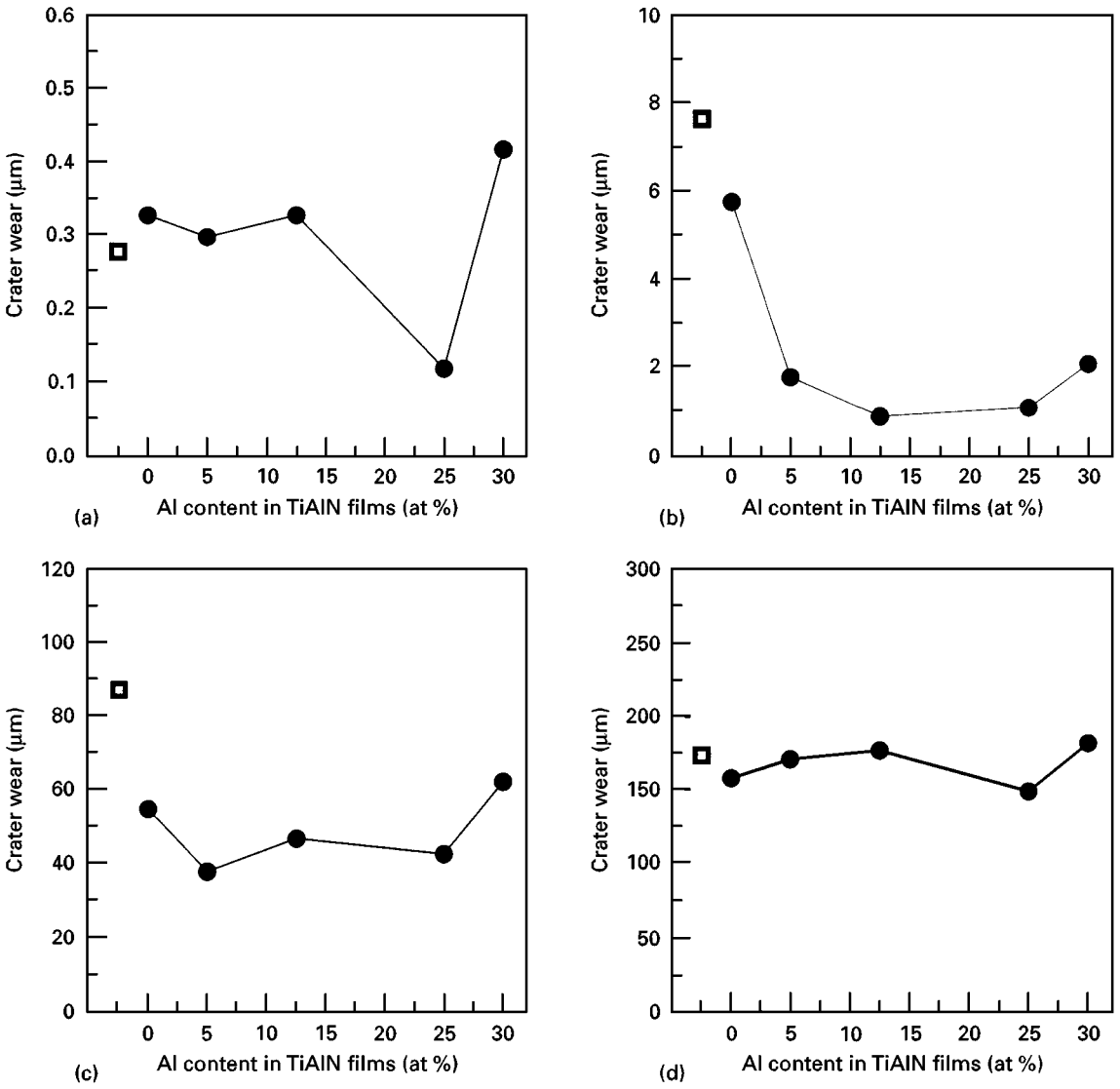

Figure 12 Crater wear depth of (●) coated and (□) uncoated tools versus the aluminium composition in TiAlN films at different cutting speeds: (a) 50 m min^{-1}, (b) 100 m min^{-1}, (c) 150 m min^{-1}, (d) 200 m min^{-1}. Cast iron was used for machining. Feed rate 0.2 mm rev^{-1}, depth of cut 1 mm, cutting distance 1640 m.

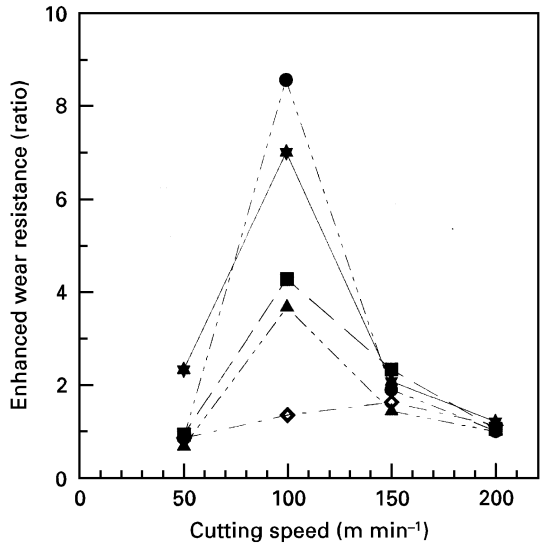

Figure 13 The enhanced wear resistance (ratio) of coated tools compared to the uncoated tools versus cutting speed. (◇) A0, (■) A5, (●) A12.5, (★) A25, (▲) A30.

tendency was quite similar to the results of hardness (Fig. 3), wear tests (Fig. 5) and diffusion of oxygen in films (Fig. 9).

Alumina has an exceptionally good chemical stability, as illustrated in Fig.10. Discussion in Section 3.4 pointed out the formation of alumina by diffusion processes at elevated cutting temperatures (Fig. 8), and that the amount of alumina consistently increased with aluminium composition (Fig. 6), except for A30, in which no crystalline phase was detected. The excellent wear resistance observed in tools containing medium aluminium was probably attributed to the formation of alumina.

4. Conclusions

1. The optimum hardness occurred at a higher nitrogen gas flow, and the value of optimum hardness also increased as the aluminium composition in TiAlN films increased. The range of nitrogen flow for obtaining optimum hardness became wider as the composition of aluminium in targets increased.

2. The optimum hardness, wear resistance, and oxidation resistance occurred as the aluminium in TiAlN reached a critical value. This was probably correlated to the chemical stability and wear property of oxidation phases formed at cutting temperatures. The formation of alumina due to the counter diffusion of aluminium and oxygen in films, had a particularly substantial effect on the crater wear resistance of tools.

3. The lattice parameter and valence electron concentration in TiAlN films decreased linearly with increasing aluminium composition which indicates the substitution of the relatively smaller aluminium by titanium atoms.

4. An oxidation test conducted at 800 °C for 1 h indicated that the amount of alumina increased, and TiO_2 gradually converted into TiO with increasing aluminium content. When the aluminium content exceeded a critical value, however, no crystalline phases were detected. A substantial amount of iron oxide was detected in samples without TiAlN coating.

5. The adhesive strength of TiAlN films decreased with increasing aluminium content.

6. The improvement of cutting performance due to the coating was a function of cutting speed and aluminium composition. An optimum improvement of nine times in the crater wear resistance was observed at 100 and 150 m min^{-1}.

Acknowledgements

The author thanks the National Science Council of Taiwan for its financial support under contract no. NSC 84-2216-E012-001, Professor J. L. Huang and Dr B. Y. Shew (National Cheng-Kung University, Tainan, Taiwan) for their help to finish this work.

References

1. O. KNOTEK and T. LEYENDECKER, *J. Solid State Chem.* **70** (1987) 318.
2. WOLF-DIETER MUNZ, *J. Vac. Sci. Technol.* **A4** (1986) 2717.
3. W. KONIG, R. FRITSCH and D. KAMMERMEIER, *Surf. Coatings Technol.* **49** (1991) 316.
4. R. KOMANDURI and J. D. DESAI, *Carbide Tool J.* January/February, Vol. **16** (1984) 3.
5. O. KNOTEK, W. D. MUNZ and T. LEYENDECKER, *J. Vac. Sci. Technol.* **A5** (1987) 2173.
6. T. LEYENDECKER, O. LEMMER, S. ESSER and J. EBBERINK, *Surf. Coatings Technol.* **48** (1991) 175.
7. G. HAKANSSON, J.-E. SUNDGREN, D. McINTYRE, J. E. GREENE and W.-D. MUNZ, *Thin Solid Films*, **153** (1987) 55.
8. H. A. JEHN, S. HOFMANN, V.-E. RUCKBORN and W.-D. MUNZ, *J. Vac. Sci. Technol.* **A4** (1986) 2701.
9. D. McINTYRE, J. E. GREENE, G. HAKANSSON, J.-E. SUNDGREN and W.-D. MUNZ, *J. Appl. Phys.* **67** (1990) 1542.
10. H. FRELLER and H. HAESSLER, *Thin Solid Films* **153** (1987) 67.
11. J. R. ROOS, J. P. CELIS, E. VANCOILLE, H. VELTROP, S. BOELENS, F. JUNGBLUT, J. EBBERINK and H. HOMBERG, *Thin Solid Films* **193/194** (1990) 547.
12. B. Y. SHEW and J. L. HUANG, *Surf. Coatings Technol.* **71** (1995) 30.
13. B. Y. SHEW, J. L. HUANG and D. F. LII, *Thin Solid Films* **293** (1997) 212–219.
14. B. Y. SHEW, J. L. HUANG and D. F. LII, *J. Mater. Chem. Phys.* (1997) submitted.
15. B. Y. SHEW and J. L. HUANG, *Surf. Coatings Technol.* **73** (1995) 66.
16. P. K. MEHROTRA and D. T. QUINTO, *J. Vac. Sci. Technol. A*, **3** (1985) 2401.
17. J. GARY BALDONI and S. T. BULJAN, *Ceram. Bull.* **67** (2) (1988) 381–387.
18. J. MUSIL, S. KADLEC, J. VYSKOCIL and V. VALVODA, *Thin Solid Films* **167** (1988) 107.
19. V. VALVODA, R. KUZEL and R. CERNY, *ibid.* **156** (1988) 53.
20. U. KONIG, *Surf. Coatings Technol.* **33** (1987) 91.
21. S. V. SUBRAMANIAN, S. S. INGLE and D. A. R. KAY, *ibid.* **61** (1993) 293.
22. R. S. COWAN and W. O. WINER, in "ASM Handbook", Vol. 18, "Friction, Lubrication and Wear Technology", edited by P. Blau, (ASM International, Materials Park, OH (1992) pp. 39–44.
23. D. McINTYRE, J. E. GREENE, G. HAKANSSON, J.-E. SUNDGREN and W.-D. MUNZ, *J. Appl. Phys.* **67** (1990) 1542.

24. SIEGFRIED HOFMANN and HERMANN, A. JEHN, *Surf. Interface Anal.* **12** (1988) 329.
25. J. R. ROOS, J. P. CELIS, E. VANCOILLE, H. VELTROP, S. BOELENS, F. JUNGBLUT, J. EBBERINK and H. HOMBERG, *Thin Solid Films* **193/194** (1990) 547.
26. B. M. KRAMER and P. K. JUDI, *J. Vac. Sci. Technol.* **A3** (1985) 2439.
27. MILTON C. SHAW, in "Metal Cutting Principles" (Clarendon Press, Oxford, 1984) Ch. 12.
28. E. RABINOWICZ, *Lubr. Eng.* **33** (1977) 378.
29. R. KOMANDURI and J. D. DESAI, *Carbide Tool J.* September/October, Vol. **15** (1983) 3.
30. MILTON C. SHAW, in "Metal Cutting Principles" (Clarendon Press, Oxford, 1984) Ch. 11, pp. 234–35.

Received 27 November 1996
and accepted 5 December 1997